Relation between Single Neuron and Population Spiking Statistics and Effects on Network Activity

Hideyuki Câteau[1,2] and Alex D. Reyes[1]

[1]*Center for Neural Science, New York University, 4 Washington Place, New York, New York 10003, USA*
[2]*RIKEN Brain Science Institute, 2-1 Hirosawa, Wako, Saitama 351-0198, Japan*

(Received 5 July 2005; published 6 February 2006)

To simplify theoretical analyses of neural networks, individual neurons are often modeled as Poisson processes. An implicit assumption is that even if the spiking activity of each neuron is non-Poissonian, the composite activity obtained by summing many spike trains limits to a Poisson process. Here, we show analytically and through simulations that this assumption is invalid. Moreover, we show with Fokker-Planck equations that the behavior of feedforward networks is reproduced accurately only if the tendency of neurons to fire periodically is incorporated by using colored noise whose autocorrelation has a negative component.

DOI: 10.1103/PhysRevLett.96.058101 PACS numbers: 87.19.La, 02.50.Ey, 05.10.Gg, 87.18.Sn

Neurons have a variety of ion channels that transduce synaptic input into spiking output. Because the channels have a wide range of activation time constants (submilliseconds to seconds), whether or not an input will generate a spike depends substantially on the recent history of the neuron. Injection of steady and/or white noise current will cause the neurons to fire in a quasiregular fashion [Fig. 1(a), left], as evidenced by the nonexponential interspike interval (ISI) distribution (middle) and the presence of multiple peaks and troughs in the autocorrelation (AC) of the spikes (right). These *in vitro* observations coupled with careful analyses of *in vivo* spiking patterns indicate that neurons are fundamentally not Poisson processes [1] (see also Ref. [2]). Nevertheless, to facilitate theoretical treatment of large-scale networks, the composite activity obtained by summing the spikes of the individual neurons in a network is often assumed to be Poissonian or Gaussian, particularly if the number of neurons is large. However, we show here by using Fokker-Planck equations (FPEs) [3] to model feedforward neural networks that this assumption leads to significant errors. Synchrony, shown experimentally to develop in such networks, is accurately reproduced only with a modified FPE that uses noise whose AC has a negative component, similar to what occurs in real neurons.

In the following, we consider a network of leaky integrate-and-fire (LIF) neurons arranged in a feedforward fashion (Fig. 2, inset). Feedforward networks have been examined experimentally [4] and so can be used to validate the results of the simulations and theory. The LIF evolution, before crossing threshold, is described by

$$\tau_m \frac{dv}{dt} = -v - G(t)(v - V_E). \quad (1)$$

where $\tau_m = 20$ ms is the membrane time constant, v is membrane potential, V_E is the reversal potential for excitatory synaptic input, and $G(t)$ is the total conductance generated by the presynaptic input neurons. A neuron in a given layer receives input from 44 out of 1000 neurons from the previous layer.

During a stimulus, the total input to each neuron is a sum of the individual spike trains, $s_j(t)$, of the presynaptic cells: $s(t) = s_1(t) + \cdots + s_N(t)$. Each spike generates a unitary conductance change in the postsynaptic neurons, $\bar{G}\tau_s \eta(t)$, where $\eta(t) = \Theta(t)\frac{1}{\tau_s} e^{-t/\tau_s}$ [$\Theta(t)$ is the Heaviside step

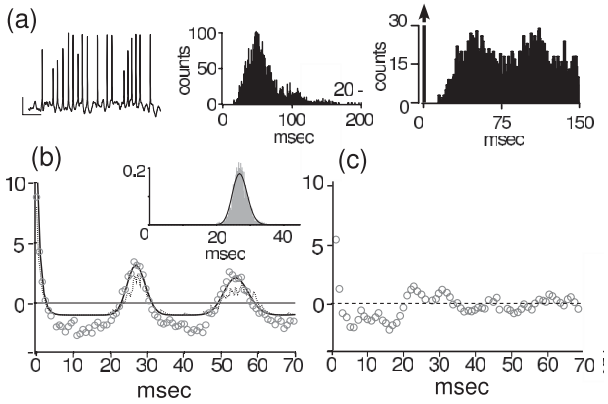

FIG. 1. Autocorrelation of single and composite spike trains. (a) left: Spike trains recorded intracellularly from a repetitively firing neuron using an *in vitro* slice preparation at rat cortex. Neurons were made to fire with input that mimicked synaptic barrages; see Ref. [4]. Scale bars: vertical = 20 mV, horizontal = 200 ms. Middle: interspike interval distribution compiled over repeated stimulation of the neuron. Right: autocorrelation of the spike trains. (b) Superimposed traces of normalized conductance autocorrelation calculated analytically with Eq. (3) (solid line) and with simulations of LIF neurons with a single input ($G_1(t)$) (dashed line) and with $N = 44$ inputs [$G(t)$ divided by N] (circles). Inset shows the interspike distribution of LIF neurons [see Fig. 2(a)] fitted with a gamma distribution ($\theta = 150$ and $\lambda = 37$ Hz). (c) Normalized autocorrelation of the conductance for a heterogeneous population of neurons. We use 44 gamma distributions with λ varying randomly between 26 and 48 Hz to generate multiple spike trains.

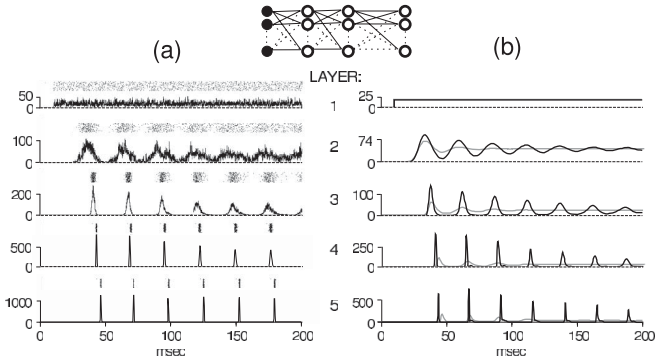

FIG. 2. Simulated and predicted behavior of feedforward networks. (a) Dot rasters and associated histograms for the first five layers of a simulated feedforward network. Note that full synchrony develops after the third layer and is maintained for the duration of the stimulus (200 ms). (b) Probability distributions calculated using Fokker-Planck equations with Poisson, Eq. (9), (gray line) and colored (black line) noise, Eq. (13), with $\alpha = 0.8$.

function], $\bar{G} = 0.20$, and the synaptic time constant, $\tau_s = 1$ ms. Using Eq. (1), these values result in a single excitatory postsynaptic potential with an amplitude of 0.6 mV, comparable to what has been measured experimentally [5]. To stimulate the network, the firing rate of first layer neurons is stepped to 37 Hz at $t = 10$ ms from a baseline rate of 1 Hz. This causes v of second layer neurons to rise. Upon crossing that threshold, v is reset to -3 mV. This cycle can repeat several times during the stimulus.

The ISI distribution of LIF neurons resembles that of real neurons [Fig. 1(a), middle] and is well described with a gamma distribution: $f_{\theta,\nu}(t) = \frac{\nu}{(\theta-1)!}(\nu t)^{\theta-1}e^{-\nu t}$. If the ISIs are randomly sampled from this distribution with $\nu = \lambda\theta$ and with $\lambda(t)$ changing much slower than τ_s, the AC of $G(t)$ is given by

$$\langle\langle G_1(t+T)G_1(t)\rangle\rangle = (\bar{G}\tau_s)^2\lambda(t)\kappa(T, \lambda(t)) \qquad (2)$$

where

$$\kappa(T,\lambda) = \frac{1}{2\tau_s}e^{-|T|/\tau_s} + \frac{1}{2\tau_s}\int_{-\infty}^{\infty} dx Q(x,\lambda)e^{-|x-T|/\tau_s} - \lambda \qquad (3)$$

with $Q(t, \lambda) = f_{\theta,\theta\lambda}(t) + f_{\theta,\theta\lambda} * f_{\theta,\theta\lambda}(t) + \cdots$ [6]. Single angular brackets $\langle A(t)\rangle$ signify the ensemble average and double angular brackets the relative correlation: $\langle\langle A(t_1)B(t_2)\rangle\rangle = \langle A(t_1)B(t_2)\rangle - \langle A(t_1)\rangle\langle B(t_2)\rangle$.

The normalized AC, $\langle\langle G_1(t+T)G_1(t)\rangle\rangle/(\langle G_1(t+T)\rangle \times \langle G_1(t)\rangle)$, calculated from LIF simulations [Fig. 1(b), dashed lines], matches the plot of $\kappa(T, \lambda)/\lambda$ versus T [Fig. 1(b), solid line]. Both are marked by troughs that flank a central peak followed by troughs and progressively decreasing peaks.

A common misconception is that summing the spikes from a large population of uncorrelated neurons results in a composite train [$S(t)$] that is Poisson. However, the expression for the AC of the composite spike trains [Eq. (4)] shows that if the firing of individual neurons are uncorrelated, the cross terms vanish and the AC reduces to that of a single spike train:

$$\begin{aligned}\langle\langle s(t+T)s(t)\rangle\rangle &= \langle\langle (s_1(t+T) + \cdots + s_N(t+T)) \\ &\quad \times (s_1(t) + \cdots + s_N(t))\rangle\rangle \\ &= \sum_i \langle\langle s_i(t+T)s_i(t)\rangle\rangle + \sum_{i\neq j}\langle\langle s_i(t+T)s_j(t)\rangle\rangle \\ &= N\langle\langle s_1(t+T)s_1(t)\rangle\rangle \qquad (4)\end{aligned}$$

The expression for conductance then becomes

$$\begin{aligned}\langle\langle G(t+T)G(t)\rangle\rangle &= N\langle\langle G_1(t+T)G_1(t)\rangle\rangle \\ &= (\bar{G}\tau_s)N\lambda(t)\kappa(T,\lambda). \qquad (5)\end{aligned}$$

Note that if $s(t)$ is Poissonian, $\langle\langle s(t+T)s(t)\rangle\rangle \propto \delta(T)$ and $\langle\langle G(t+T)G(t)\rangle\rangle \propto \exp(-T/\tau_s)$. However, the right-hand side of Eq. (5) never limits to the single-exponential function as $N \to \infty$; a double limit of $\lambda \to 0$ and $N \to \infty$ with $N\lambda$ kept constant is required. These limits are unlikely to hold under physiological conditions because a reasonable value of λ is needed for signals to propagate through the network [4].

Simulations confirm that the AC of the summated conductance $G(t) = G_1(t) + \cdots + G_N(t)$, divided by N [Fig. 1(b) circles], matches $\langle\langle G_1(t+T)G_1(t)\rangle\rangle$ (dashed line). Both ACs are normalized [divided by $\langle G_1(t+T)\rangle \times \langle G_1(t)\rangle$]. The sparse connectivity in the network ensured that the correlation between neurons were low so that the cross terms in Eq. (4) vanish; the cross terms would contribute more if neurons shared significant inputs from the previous layer.

Increasing the heterogeneity of the network does not eliminate the primary trough of the AC. Figure 1(c) (circles) shows the composite AC compiled for 44 spike trains whose firing rates are randomized between 26 and 48 Hz. The main effect of increasing heterogeneity is to smear out later troughs and peaks, with minimal effects on the primary trough.

Note that since the calculation of the AC of the total conductance reduces to that of the conductance induced by a single neuron [Eq. (5)], the AC of the total conductance therefore does not vary with N and becomes a delta function only if ACs of the individual conductances are themselves delta functions. ''Whitening'' of conductance noise can occur only under special conditions such as when the average firing rate of each neuron is very low (which stretches and flattens the AC), or if neurons exhibit bursting behaviors.

To determine how the non-Poissonian spiking of individual neurons is manifested in the network activity, we compared the behavior predicted with FPE using white noise (FPE_W) [7,8] with that predicted with FPE using colored noise whose AC has a trough (FPE_C). The FPE provides us with a quasianalytical tool to analyze firing pattern of population of neurons. Compared to a direct simulation method, a quasianalytical method gives a clearer insight into the underlying mechanism of the phenomena.

A salient feature of feedforward networks, as revealed experimentally [4] and by simulations [Fig. 2(a)] [9] (see also Ref. [10]), is that the firing of neurons in successive layers become progressively more synchronous [Fig. 2(a)].

For Poissonian spike trains, the first 2 moments are given by $\langle s(t)\rangle = N\lambda(t)$ and $\langle\langle s(t+T)s(t)\rangle\rangle = N\lambda(t)\delta(T)$. The associated moments for conductance are given by

$$\langle G(t)\rangle = \bar{G}\tau_s N\lambda(t) \tag{6}$$

and

$$\langle\langle G(t+T)G(t)\rangle\rangle = (\bar{G}\tau_s)^2 N\lambda(t)\frac{1}{2\tau_s}e^{-|T|/\tau_s}. \tag{7}$$

This leads to an approximate representation of the conductance in terms of Gaussian white noise, $w(t)$:

$$G(t) \cong \bar{G}\tau_s(N\lambda(t) + \sqrt{N\lambda(t)}w(t)) \tag{8}$$

under the condition that $\tau_s \ll \tau_m$ [11]. Combining with Eq. (1) gives a stochastic differential equation and the FPE [7,12]:

$$\frac{\partial p(u,t)}{\partial t} = -\frac{\partial}{\partial u}a(u,R)p + \frac{b(R')^2}{2}\frac{\partial^2 p}{\partial u^2} + J_u(t)\delta(u - U_{\text{reset}}). \tag{9}$$

where $a(u,R) = (\bar{G}\tau_s R + 1 - e^u)/\tau_m$ and $b(R') = (\bar{G}\tau_s/\tau_m)\sqrt{R'}$.

To account for the finite time course of synaptic conductance without compromising mathematical tractability, we replaced the input rate term, $N\lambda$, in drift and diffusion terms with $R = N\lambda * \eta$ and $R' = N\lambda * \eta_2$ with $\eta_2(t) = \Theta(t)2/\tau_s \exp(-2t/\tau_s)$ [8]. For convenience, v is transformed to $u = \ln(V_E/(V_E - v))$. The probability flux term, $J_u(t) = -\frac{\partial p}{\partial u}|_{u=\text{thresold}}$, ensures that the probability sum is time invariant. Because the flux term represents the portion of the population voltage that exceeded threshold and is subsequently reset to U_{reset}, its value gives the total number of neurons that fire at a given time.

A copy of the FPE is prepared for each layer (except layer 1) and solved simultaneously. The rates calculated with the FPE [Fig. 2(b), gray line] do not match the histograms given by the simulations [Fig. 2(a)]. Although there are peaks that repeat in time, each successive peak broadens and eventually flattens.

The FPE with non-Poissonian noise is constructed as follows [12]. The expression for conductance [Eq. (4)] can be modified for colored noise, $L_1(t)$:

$$G(t) = \bar{G}\tau_s(N\lambda(t) + \sqrt{N\lambda(t)}L_1(t)) \tag{10}$$

where $\langle L_1(t)\rangle = 0$ and $\langle L_1(t)L_1(0)\rangle = \kappa(t,\lambda)$.

For small τ_s, $L_1(t)$ may be expressed in terms of the standard Gaussian white noise $w(t)$ by introducing auxiliary variable, X:

$$L_1(t) \equiv w(t) - \alpha X(t),$$
$$\tau_{\text{neg}}dX/dt = -X + w(t). \tag{11}$$

Formal integration yields an expression

$$\langle L_1(t)L_1(0)\rangle = \delta(t) - \frac{\beta}{2\tau_{\text{neg}}}e^{-|t|/\tau_{\text{neg}}} \tag{12}$$

that resembles $\kappa(t,\lambda)$. The time constant of the negative component, τ_{neg}, is set to be proportional to the average ISI of presynaptic neurons and $\beta = 1 - (1-\alpha)^2$. Equation (12) reproduces only the 1st negative component and not the subsequent peaks and troughs of the LIF neurons' AC, similar to the AC of the heterogeneous network [Fig. 1(c)].

These stochastic equations differ from those used previously [13] where the noise is colored by making the synaptic time course longer ($\tau_s \neq 0$): $w(t)$ appeared only in the lower expression of Eq. (11), so that the AC of the noise had an exponentially decaying peak but not a negative trough component.

The new FPE derived from standard procedures [3] is given by

$$\frac{\partial P(u,X,t)}{\partial t} = -\frac{1}{\tau_m}\frac{\partial}{\partial u}\left(\tau_m a(u,R+R_0) - \bar{G}\tau_s\sqrt{R'}\left(\alpha X + \frac{1}{\tau_{\text{neg}}}\frac{\partial}{\partial X}\right)\right)P + \frac{b(R'+R_0+R_1)^2}{2}\frac{\partial^2 P}{\partial u^2} + \frac{1}{\tau_{\text{neg}}}\frac{\partial(XP)}{\partial X}$$
$$+ \frac{1}{2\tau_{\text{neg}}{}^2}\frac{R'+R_1}{R'}\frac{\partial^2 P}{\partial X^2} + J_u(X,t)\delta(u - U_{\text{reset}}) \tag{13}$$

with $\tau_{\text{neg}} = 1/(2\lambda)$. Detailed derivation of this equation as well as the algorithm for numerical integration is found in the supplementary material [14]. To suppress instability in the numerical integration of the two dimensional Fokker-Planck equation, we added two noise sources whose input rates, $R_0 = R_1 = N \times 3$ Hz, are much lower than the input rate from the previous layer ($= N \times 37$ Hz). This noise was also included in the simulations and in the calculations with FPE_W. Although the stationary solution to Eq. (13) can be used to analytically calculate the steady-state firing rate [12], calculation of the time-varying distribution required numerical integration using the alternating difference implicit algorithm [15].

The firing rates calculated using FPE_C reproduced the histograms obtained with the simulations [Fig. 2(b), black line] more accurately than those calculated using FPE_W (gray line). Unlike with FPE_W, the FPE_C produced distributions that did not flatten rapidly with time. With the FPE_W, the firings times easily diverges to a nonstructured firing pattern; those obtained with FPE_C tended to remain periodic with the FPE_C. Those effects are readily understandable from the AC, which provides information about the timing of spikes. FPE_C provided better matches partly because the negative component in the AC means that spikes tend to occur at a fixed delay from the previous spike [16], unlike a Poisson process where the spike times

are independent of previous events. As a result, the spikes are tightly clustered around one interspike interval, whereas spikes of a Poisson process are considerably more dispersed. This increased regularity in firing sharpened the histogram peaks.

As shown previously, the FPE_W accurately describes [8] the propagation of a brief packet of input through a feedforward synfire chain [17]. Because each neuron in the layer contributes only one spike, the negative component of the AC plays no role. The FPE_C should be used for longer duration stimulus where cells can fire multiple times. It should be noted, however, that the peaks of the FPE_C predicted rates are most accurate mainly for the first 200–300 ms; at longer intervals, the rates flatten out whereas the histograms with the simulations remain sharp (data not shown). Simulations suggest that this discrepancy likely arises from the fact that the AC of the colored noise had only the central peak and side troughs, unlike those of the simulated (Fig. 1) and real (e.g., [18]) neurons, which exhibit multiple peaks and troughs. Relaxing this assumption, however, makes calculation of FPE intractable.

At the most basic level, neurons are not Poisson processes. Thus, the occurrence of a spike will depend substantially on the recent firing history. Indeed, it is difficult to force neurons to fire in a Poisson manner [4]. Our analyses suggest that firing statistics of individual neurons can greatly affect the behavior of the network. An important consequence of non-Poissonian firing is that any temporal correlation in the firing of neurons at the onset of a sensory input is likely to be maintained for the duration of the stimulus. This, coupled with the fact that neurons respond differently to synchronous and asynchronous input [19], is likely to greatly affect signal processing at the network level. The predictions obtained with Poisson processes are likely to differ substantially from formulations that incorporate the realistic firing statistics of neurons.

This work is supported by NSF Grant No. IBN-0079619, by NIH Grant No. DC005787-01A1 and No. NEI-13145, and the EJLB Foundation. We thank B. Doiron, D. Tranchina, D. Cai, J. Simon, and S. Fusi for helpful discussions and K. Kitano for help with a simulation code.

[1] C. F. Stevens and A. M. Zador, Nat. Neurosci. **1**, 210 (1998); Y. Sakai, S. Funahashi, and S. Shinomoto, Neural Networks **12**, 1181 (1999); Y. Sakai, Neural Networks **14**, 1145 (2001); S. Shinomoto and Y. Tsubo, Phys. Rev. E **64**, 041910 (2001); J. Feng and P. Zhang, Phys. Rev. E **63**, 051902 (2001); E. Salinas and T. J. Sejnowski, Neural Comput. **14**, 2111 (2002); S. Shinomoto, K. Shima, and J. Tanji, Neural Comput. **15**, 2823 (2003).

[2] M. N. Shadlen and W. T. Newsome, J. Neurosci. **18**, 3870 (1998).

[3] H. Risken, *The Fokker-Planck Equation* (Springer-Verlag, New York, 1996).

[4] A. D. Reyes, Nat. Neurosci. **6**, 593 (2003).

[5] A. D. Reyes and B. Sakmann, J. Neurosci. **19**, 3827 (1999).

[6] F. Gabbiani and C. Koch, in *Principles of Spike Train Analysis*, edited by C. Koch and I. Segev, Methods in Neuronal Modeling (MIT Press, Cambridge, Masschusetts, 1998).

[7] B. W. Knight, J. Gen. Physiol. **59**, 734 (1972); W. J. Wilbur and J. Rinzel, Biol. Cybern. **45**, 107 (1982); L. F. Abbott, and C. van Vreeswijk, Phys. Rev. E **48**, 1483 (1993); W. Gerstner, Phys. Rev. E **51**, 738 (1995); N. Brunel and V. Hakim, Neural Comput. **11**, 1621 (1999); A. Omurtag, B. W. Knight, and L. Sirovich, J. Comput. Neurosci. **8**, 51 (2000); D. Q. Nykamp and D. Tranchina, J. Comput. Neurosci. **8**, 19 (2000); N. Brunel, J. Comput. Neurosci. **8**, 183 (2000); B. Lindner and L. Schimansky-Geier, Phys. Rev. Lett. **86**, 2934 (2001); H. Câteau and T. Fukai, Neural Comput. **15**, 597 (2003); T. Kanamaru and M. Sekine, Phys. Rev. E **67**, 031916 (2003); M. Rudolph and A. Destexhe, Neural Comput. **15**, 2577 (2003); N. Masuda and K. Aihara, Neural Comput. **15**, 1341 (2003); H. Meffin, A. N. Burkitt, and D. B. Grayden, J. Comput. Neurosci. **16**, 159 (2004); E. Brown *et al.*, J. Comput. Neurosci. **17**, 13 (2004); B. Doiron *et al.*, Phys. Rev. Lett. **93**, 048101 (2004); N. Masuda and K. Aihara, Neural Comput. **16**, 627 (2004); K. Hamaguchi, M. Okada, and K. Aihara, Adv. Neural Inf. Proc. Syst. **17**, 553 (2005); N. Masuda, Neural Comput. **18**, 45 (2006).

[8] H. Câteau and T. Fukai, Neural Networks **14**, 675 (2001).

[9] V. Litvak *et al.*, J. Neurosci. **23**, 3006 (2003).

[10] M. C. van Rossum, G. G. Turrigiano, and S. B. Nelson, J. Neurosci. **22**, 1956 (2002); N. Masuda and K. Aihara, Phys. Rev. Lett. **88**, 248101 (2002); Y. Sakai, BioSystems **67**, 221 (2002); N. Masuda and K. Aihara, Neural Comput. **15**, 103 (2003).

[11] S. Hestrin, P. Sah, and R. Nicoll, Neuron **5**, 247 (1990).

[12] R. Moreno-Bote *et al.*, Phys. Rev. Lett. **89**, 288101 (2002).

[13] N. Brunel and S. Sergi, J. Theor. Biol. **195**, 87 (1998); G. Svirskis and J. Rinzel, Biophys. J. **79**, 629 (2000); D. Q. Nykamp and D. Tranchina, Neural Comput. **13**, 511 (2001); E. Haskell, D. Q. Nykamp, and D. Tranchina, Network **12**, 141 (2001); N. Fourcaud and N. Brunel, Neural Comput. **14**, 2057 (2002); D. Cai *et al.*, Proc. Natl. Acad. Sci. U.S.A. **101**, 7757 (2004); R. Moreno-Bote and N. Parga, Phys. Rev. Lett. **92**, 028102 (2004); R. Moreno-Bote and N. Parga, *ibid.* **94**, 088103 (2005).

[14] See EPAPS Document No. E-PRLTAO-96-039606 for details regarding Eq. (13). For more information on EPAPS, see http://www.aip.org/pubservs/epaps.html.

[15] W. Morton, *Numerical Solution of Partial Differential Equation* (Cambridge University Press, Cambridge, 1994).

[16] D. J. Mar *et al.*, Proc. Natl. Acad. Sci. U.S.A. **96**, 10 450 (1999).

[17] M. Abeles *et al.*, J. Neurophysiol. **70**, 1629 (1993); A. N. Burkitt and G. M. Clark, Neural Comput. **11**, 871 (1999); M. Diesmann, M. O. Gewaltig, and A. Aertsen, Nature (London) **402**, 529 (1999); J. M. Beggs and D. Plenz, J. Neurosci. **23**, 11 167 (2003); K. Hamaguchi *et al.*, Neural Comput. **17**, 2034 (2005).

[18] H. Kita *et al.*, J. Neurophysiol. **92**, 3069 (2004).

[19] A. D. Reyes and E. E. Fetz, J. Neurophysiol. **69**, 1673 (1993); A. D. Reyes and E. E. Fetz, *ibid.* **69**, 1661 (1993); Oviedo and Reyes, Nat. Neurosci. **5**, 261 (2002).

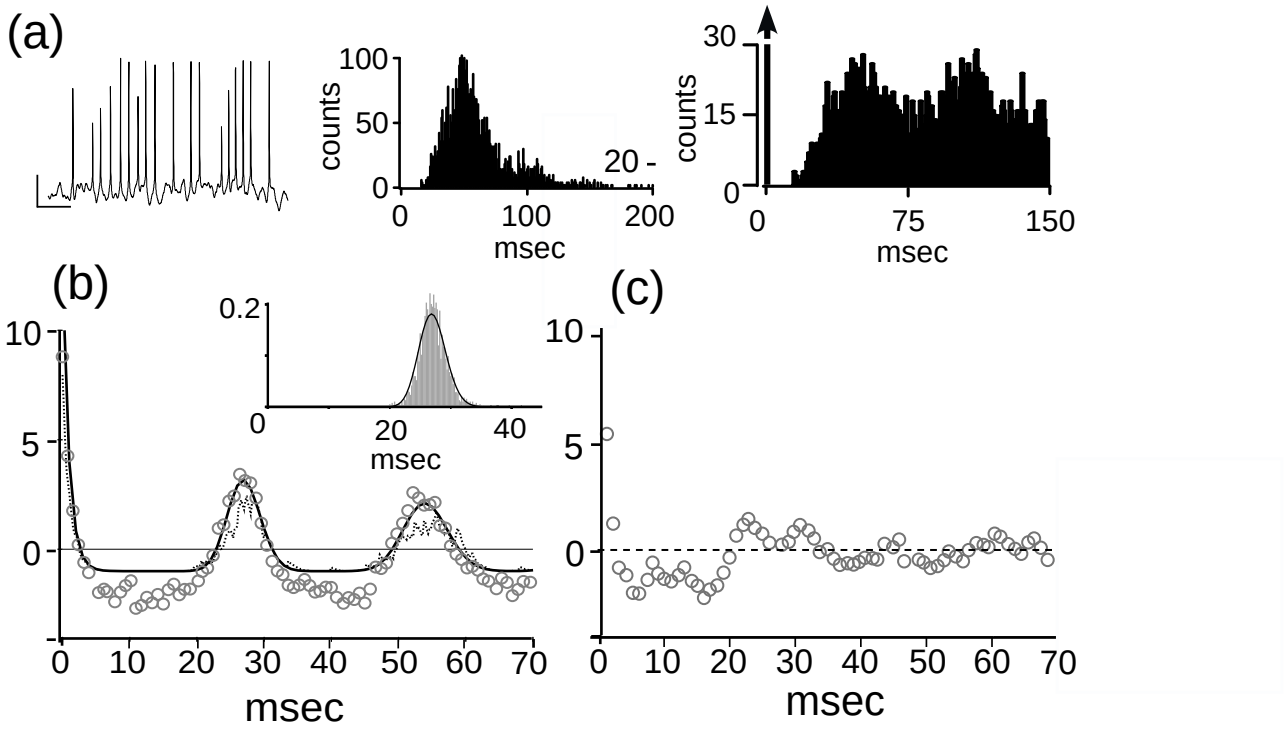
(a)
100
50
0
counts
20 -
0
100
200
msec
30
15
0
counts
0
75
150
msec
(b)
0.2
0
20
40
msec
10
5
0
0
10
20
30
40
50
60
70
msec
(c)
10
5
0
0
10
20
30
40
50
60
70
msec

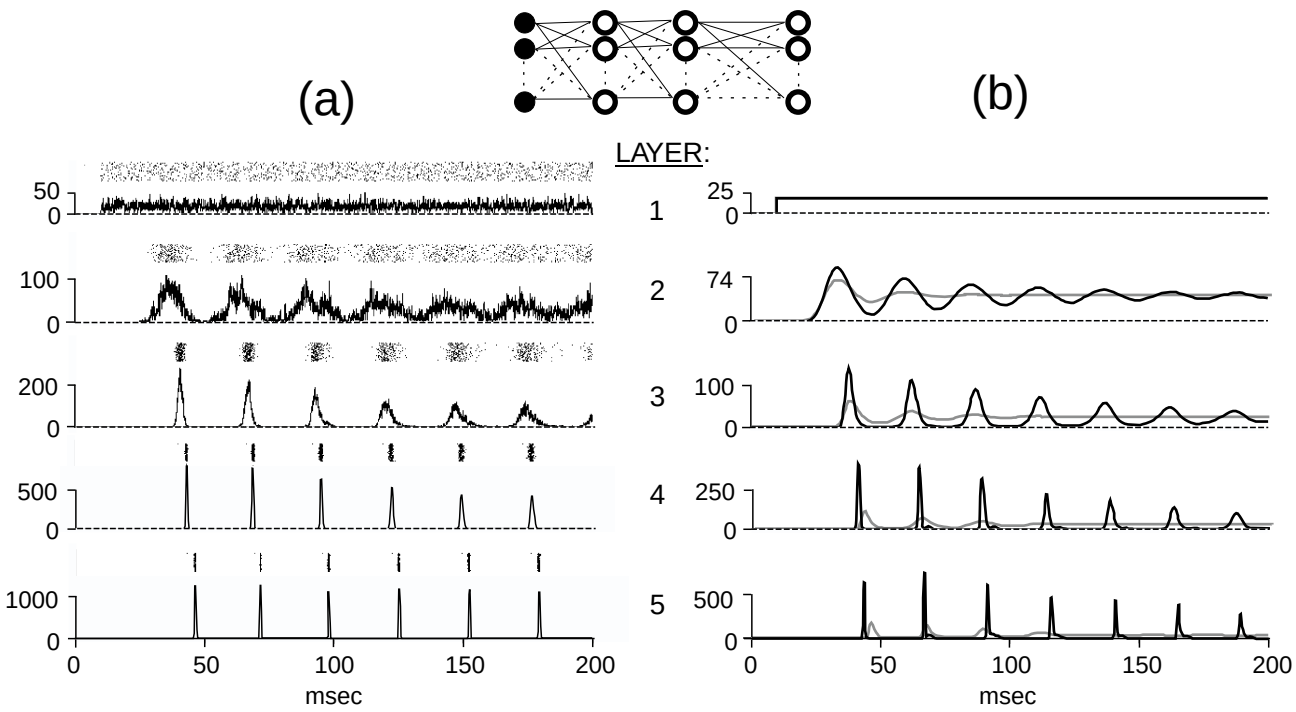
(a)
(b)
LAYER:
50
0
100
0
200
0
500
0
1000
0
0
50
100
150
200
msec
1
25
0
2
74
0
3
100
0
4
250
0
5
500
0
0
50
100
150
200
msec